HHS Public Access

Author manuscript

Neuroimage. Author manuscript; available in PMC 2019 September 01.

Published in final edited form as:

Neuroimage. 2018 September ; 178: 713–720. doi:10.1016/j.neuroimage.2018.05.004.

Rodent Cerebral Blood Volume (CBV) changes during hypercapnia observed using Magnetic Particle Imaging (MPI) detection

Clarissa Zimmerman Cooley[1], **Joseph B. Mandeville**[1], **Erica E. Mason**[1,2], **Emiri T. Mandeville**[3], and **Lawrence L. Wald**[1,2]

[1]A. A. Martinos Center for Biomedical Imaging, Department of Radiology, Massachusetts General Hospital, Charlestown, MA, USA

[2]Harvard-MIT Division of Health Sciences Technology, Cambridge, MA, USA

[3]Neuroprotection Research Laboratory, Departments of Radiology and Neurology, Massachusetts General Hospital and Harvard Medical School, Boston, MA, USA

Abstract

Magnetic Particle Imaging (MPI) is a rapidly developing imaging modality that directly measures and maps the concentration of injected superparamagnetic iron oxide nanoparticles (SPIOs). Since the agent does not cross the blood-brain barrier, cerebral SPIO concentration provides a direct probe of Cerebral Blood Volume (CBV). Here we provide an initial demonstration of the ability of MPI to detect functional CBV changes (fCBV) by monitoring SPIO concentration during hypercapnic manipulation in a rat model. As a tracer detection method, MPI offers a more direct probe of agent concentration and therefore fCBV than MRI measurements in which the agent is indirectly detected through perturbation of water relaxation time constants such as T_2*. We found that MPI detection could measure CBV changes during hypercapnia with high CNR (CNR = 50) and potentially with high temporal resolution. Although the detection process more closely resembles a tracer method, we also identify evidence of physiological noise in the MPI time-series, with higher time-series variance at higher concentration levels. Our findings suggest that CBV-based MPI can provide a detection modality for hemodynamic changes. Further investigation with tomographic imaging is needed to assess tomographic ability of the method and further study the presence of time-series fluctuations which scale with signal level similar to physiological noise in resting fMRI time-courses.

Keywords

Magnetic Particle Imaging; Iron oxide Nanoparticles; Cerebral Blood Volume; Hypercapnia

1. Introduction

In this work, we investigate the feasibility of Magnetic Particle Imaging (MPI) as an alternative functional neuroimaging modality to functional MRI for detection of hemodynamic modulations. While MRI is a versatile imaging method capable of measuring *in vivo* hemodynamic changes associated with brain activation, the CNR of fMRI remains problematically low. Low CNR can lead to low detection rates of subtle activations in task-based studies and weak or missed network connections in functional connectivity studies. In response, it is common to use group averaging to uncover population effects, which limits the utility of fMRI for individualized medicine to only the strongest activation paradigms and most robust resting-state networks.

Iron oxide nanoparticle contrast agents are widely used in preclinical/translational fMRI experiments to increase sensitivity and spatial specificity compared to endogenous contrast sources such as BOLD [1]–[5]. Used as a blood-pool agent, iron oxide nanoparticles provide an indirect reporter of CBV changes through the relationship between the voxel's iron concentration (and thus blood content) and the local T_2* relaxation rate. CBV methods have also been shown to improve CNR in human functional imaging experiments using Ferumoxytol [6]–[8]. Additionally, CBV-based fMRI has been shown to better localize brain activation [9]–[11]. But, direct quantification of CBV changes during activation using SPIO facilitated MRI measurements is complicated by the simultaneous signal increases caused by the BOLD effect, which partially cancels the signal decreases induced by the CBV increase during activation [3].

Although use of iron oxide blood-pool agents increases fractional signal changes in response to CBV changes and therefore improves CNR, there is still need for improvement. In this work, we investigate the use of Magnetic Particle Imaging (MPI) detection to track local iron concentrations and thus directly monitor functional CBV changes (fCBV) versus time. Cell tracking studies [12] suggest that high MPI sensitivity can be achieved, and simulation studies of rodent and human imagers [18] support the potential of MPI-based functional neuroimaging, a modality we term "fMPI." Here we attempt to experimentally validate fMPI's potential by measuring time-varying *in vivo* MPI signals during hypercapnia modulation in rodents.

MPI is an emerging imaging modality (distinct from MRI) introduced by Gleich and Weizenecker in 2005 [13]. In MPI, the signal from injected SuperParamagnetic Iron Oxide nanoparticles (SPIOs) is directly measured and mapped to form images of SPIO concentrations. While there is no magnetic resonance effect in MPI, it shares many methodological similarities with MRI. For example, the signal source is excited with an applied AC magnetic field (the "drive field") and measured by Faraday detection using receiver coils. However, unlike MRI, the alternating magnetic response originates directly from the SPIO and is measured simultaneously with the applied drive field. Since the simultaneous drive field is orders of magnitude larger than the detected fields from the magnetized iron particles, the nonlinear magnetization curve of the SPIO is leveraged to mitigate potential signal masking by the drive field. The large oscillating drive field propels the SPIO magnetization repeatedly into the saturation regime, and this nonlinear response

generates signal components at harmonics of the drive frequency. The MPI signal is derived from these harmonic components, eliminating the unwanted direct detection of flux from the drive coil. Retention of only the harmonics also ensures that MPI does not pick up linear (paramagnetic and diamagnetic) sources, enabling zero-background images. The nonlinear response also forms the basis for MPI image encoding [14], [15], which will not be discussed here since it is not used in the described experiments. Thus, the nonlinear magnetization curve of the SPIO is an essential property of MPI's signal detection.

In order to perform proof-of-concept validation of the ability of MPI to detect and ultimately map fCBV changes, we analyzed the MPI detected signal during modulation of rodent CBV from a hypercapnic challenge. We used a single-sided MP drive coil and detector to monitor changes in the detected signal at harmonics of the drive frequency. Compared to fully tomographic MPI scanners [12], [15]–[17], the single-sided MP detector is a relatively simple coil assembly which measures the detected signal within the sensitive volume immediately under the coil. The experimental results show that the blood volume changes induced by ventilated CO_2 modulation can be readily measured with high CNR using MPI detection. We also show that the detected hemodynamic signal shows the presence of "physiological noise" presumably from hemodynamic fluctuations. This suggests that it might be possible to do the equivalent of functional connectivity analysis with fMPI time-series images. These results motivate further work toward development of a full 3D fMPI scanner.

2. Materials and Methods

2.1. Instrument design

The two basic functions of the detector system are to 1) produce a low-distortion sinusoidal drive field to modulate the SPIO magnetization and 2) simultaneously and sensitively measure the 3rd harmonic component of the SPIO's magnetic response to the drive field. Figure 1 shows a schematic of our instrument, which uses a National Instrument Data Acquisition System (NI USB-6363, National Instruments Corp, Austin, TX) with MATLAB (MathWorks, Natick, MA) GUI interface as the console. This console generates the sinusoidal drive field waveform and digitizes the MPI signal from the receive chain.

Since the receive chain will be detecting small magnetization responses of SPIOs at harmonics of a single ideal drive frequency, it is important to produce a low-distortion drive field that is free of harmonics. The drive chain produces an amplitude-adjustable drive field at the surface of the rodent's skull using an AE Techron 7224 power amplifier (Elkhart, IN), a high-power 4th order low-pass filter, and a drive coil (L_{drive}), which together with the capacitance in the filter forms a series LC circuit resonant at 25 kHz. The 4th order low-pass ladder filter provides 80dB of attenuation between 25 kHz and 75 kHz in simulation. The schematic and frequency response are shown in Supplementary Figure 1. Even with this filter, some harmonic content from nonlinearities in the drive system is picked up in the receive system. Therefore, the console adds a small adjustable harmonic signal to the digitally produced drive field waveform to cancel remaining harmonic content.

The receiver system needs to overcome two challenges. First, it must be sufficiently isolated from the drive field to substantially reduce direct pickup of this field, which can saturate the preamplifier and exceed the dynamic range of the ADC. Second, it must detect the magnetization from the SPIOs with high sensitivity. To reduce the direct drive field feedthrough, a gradiometer receiver coil configuration is used (described below). The gradiometer receive coil is tuned to 75 kHz (the third harmonic of the drive frequency) as a parallel LC circuit. Additionally, a 25 kHz notch filter is used to further reduce feedthrough of the drive frequency. The resonant circuit schematic and simulated frequency response is shown in Supplementary Figure 2.

To achieve good sensitivity in the receive chain, a Stanford Research Systems SR560 (Sunnyvale, CA) low-noise preamplifier with 4nV/√Hz input noise is used to amplify the MPI signal. The parallel LC gradiometer provides a high impedance, which is nearly optimal for the preamplifier noise performance. With this configuration we expect most of the detected noise to come from copper losses in the gradiometer [18]. Finally, a second-stage high-pass filter SR650 (Stanford Research Systems, Sunnyvale, CA) is used to further attenuate 25 kHz feedthrough before console digitization. Note, the receive chain described here detects only the largest (third) harmonic of the MPI signal. While this simplifies the setup by allowing a tuned receive coil that reduces the filtering requirements, the signal power in the higher harmonics is not utilized.

Figure 2 shows a detailed schematic and photos of the detector coil assembly. The solenoid drive coil (Fig. 2b) has a 4.4 cm diameter, an 8.9 cm length, and consists of 145 turns of Litz wire (AWG 20 5/39/42) in 2 layers. This yields an inductance of 340 μH Nested inside the solenoid is the 1.7 cm diameter gradiometer receiver coil (Fig. 2c), comprised of 2 separate 1 cm long 40-turn sections wound with 24 gauge solid copper wire in opposite directions. Ideally, when the gradiometer is exactly centered in the solenoid, the voltage induced by the drive field in the gradiometer sections cancel (due to the opposing turn directions). To facilitate fine adjustment of this cancellation, a threaded rod with adjustment wheel is built into the coil assembly to adjust their relative position. Experimentally, when the gradiometer is carefully positioned, >80 dB of voltage attenuation of the drive field feedthrough is achievable.

Ohmic heating of the drive coil due to the large currents used to drive the nanoparticles requires the experiment be performed with a low duty cycle (12ms of drive current followed by 1s of rest). The experimental sensitivity could thus be improved by adding active cooling (via water or air flow) allowing a higher measurement duty cycle. Since good inductive balance is achieved by the gradiometer arrangement, relatively little current flows in the receiver circuit, but it experiences some heating through proximity to the drive coil.

2.2. Detector sensitivity profile

Unlike a full MPI scanner, the single-sided detector does not use a selection field for image encoding. Instead, we rely only on the localized sensitivity profile of the detector for signal localization. Figure 3 shows the simulated sensitivity profile under the surface of the coil assembly overlaid on an anatomical reference of a rat's head [19]. The map was generated by simulating the acquired 3rd harmonic signal from point sources of SPIO particles in a 3D

grid using an ideal Langevin model ($L(x) = \coth(x) - 1/x$). Although the detector is actually most sensitive directly under the surface (in the scalp), taking a sensitivity-weighted sum of the voxels in the brain reveals that approximately 24% of the brain is detected by the system. Assuming a brain volume of 1200 mm^3 (10.6 mm cube), 24% is equivalent to 288 mm^3 (6.5 mm cube).

2.3. Acquisition parameters

The drive field amplitude can be varied, but is typically operated to produce a 10–15 mT field at the surface of the drive coil. For these experiments, a 25 kHz sinusoidal drive field was produced in 16 ms bursts every second, during which the pre-amplified (voltage gain = 500) gradiometer voltage was concurrently sampled by the ADC at a 500 kS/s rate with a range of ±0.1 V. The initial 4 ms of the acquired data is removed to eliminate transient artifacts, and the 75 kHz component is extracted from the Discrete Fourier Transform (DFT) of the remaining 12 ms of data. Thus, each drive-field burst results in a single recorded point every second, and together these form the measured MPI time-series. Before the SPIO injection, the system is run for about 1 hr to warm up. During this warm-up period, there is a small 75 kHz signal component that drifts with thermal changes in the system and eventually stabilizes. Before beginning an experiment, the digital 75 kHz cancellation waveform generated as part of the drive-field waveform is adjusted in amplitude and phase to cancel this unwanted component to < 200 nV.

2.4. Phantom sensitivity experiment

To evaluate the sensitivity of the system, phantom experiments were conducted using PEG Carboxyl Iron Oxide Nanoparticles with a 25 nm core (SPP-25–25, Ocean Nanotech, San Diego, CA, USA). Three 18 μL bulbs were filled with different SPIO concentrations in water, containing 4.5 μg, 450 ng, and 45 ng of Fe. During a continuous time-series data set (no averaging), each sample bulb phantom was positioned at various distances from the end of the detector, **d** = [10 mm, 8 mm, 6 mm, 4 mm, 2 mm, 0 mm] (Fig. 4). Data collection began with the phantom positioned 10 cm from detector (outside detectable region). The position was alternated between each distance, **d**, and 10 cm at approximately 20 s intervals.

2.5. Animal experimental procedure

2.5.1. Animal Preparation—The animal experiments described were carried out under an approved protocol from our Institution's animal ethics committee. The animal preparation closely follows preparation used in previous fMRI CBV experiments using MION [1]. The CO_2 responsivity experiment requires full breathing control by a ventilator, necessitating a tracheostomy and use of a paralytic to avoid the animal breathing around the ventilator. Three Sprague-Dawley rats (weight 280 ± 10 g) were anesthetized with 3% isoflurane in oxygen for surgery. A tracheostomy was performed and femoral and venous cannulas were inserted. After surgery, the rats were temporarily mechanically ventilated with a mixture of 1–1.5% isoflurane in an air-oxygen mixture. After initiation of mechanical ventilation, rats were paralyzed with a 2 mg/kg bolus of pancuronium followed by continuous IV infusion at 2 mg/kg/h. Before beginning MPI experiments, isoflurane was discontinued and anesthesia was maintained with a 50 mg/kg IV bolus of α- chloralose, followed by continuous infusion

of 25 mg/kg/h. The rats were positioned on top of a heating blanket on a custom plastic bed with their front incisors inserted in an adjustable bar. The heating blanket circulated water at 40°C to maintain body temperature. The single-sided detector was positioned tightly above the rats' heads as shown in the schematic in Fig. 1.

The SPIO agent used was a 25 nm core Iron Oxide Nanoparticle with a PEG Carboxyl coating from Ocean Nanotech (San Diego, CA, USA) (same as phantom experiment). The blood half-life was measured to be approximately 1 hr in rats. The agent was diluted to 0.5 mg Fe/ml and administered as four 1.4 ml infusions at a rate of 14 ml/hr (7 mg Fe /hr). The But the total dose administered was estimated to be approximately 8.5 mg Fe/kg after correction for the dead-space in the catheter which contained dose which did not reach the animal. This dose is comparable to the typical 8–10 mg Fe/kg SPIO dose used in fMRI studies in macaques [3], and the 7 mg Fe/kg dose that has been used in humans [6], [20].

2.5.2. CO_2 responsivity—Ventilation parameters were adjusted to cycle between hypocapnia and hypercapnia in 5 minute intervals. Hypocapnia was induced with hyperventilation of normal air by raising the respiration rate to 55 breaths per minute (BPM). Hypercapnia was induced with ventilation of a 5% CO_2 air mixture at a mildly depressed respiration rate of 32 BPM. Baseline respiration rate was 34 BPM. Arterial blood samples were acquired during each state for blood gas analysis.

Continuous time-series MPI data as described above were acquired during SPIO infusion and for 4 or more cycles of hypo/hypercapnia. Data were processed with either a 0.1 Hz digital low-pass filter or no filter. For time-courses acquired after SPIO infusion, a 2nd order trend was removed from the data to account for drift and SPIO clearance.

3. Results

The single-sided MPI detector system enabled direct time-series measurements of SPIO solutions in phantoms and *in vivo.* The system was first validated with phantom experiments to determine sensitivity limits as a function of distance from the detector and SPIO concentration. Figure 4 shows voltage measurements over 13 time periods of ~20s each for the three tested SPIO concentrations at 7 distances from the detector. Assuming a 5% blood concentration, we estimate that a 3 mm voxel in the brain contains 1.35 μl of blood. For a 10mg Fe /kg SPIO dose in a 300 g rat with 64 ml/kg of total blood volume, a voxel with 5% CBV contains 211 ng Fe. Therefore, to detect a 25% neuroactivation-induced CBV change in this voxel, the detector must be sensitive to 53 ng Fe. Our results show that we can detect a 45 ng Fe sample at the surface of the detector with an SNR of about 5.4, indicating the ability to detect this 25% hemodynamic change at the surface of the detector without averaging. The signal level for the 3 samples scales roughly linearly with the Fe concentration in the sample, validating the ability to make quantitative measurements with MPI detector.

Figures 5–7 show *in vivo* MPI data from the single-sided detector positioned closely over the anesthetized rat's head. Figure 5a shows the raw time-series data during the four SPIO infusions in rat #1. All four 1.4 mg Fe infusions were administered at the same rate (7 mg

Fe/hr). The approximately linear increase of SPIO in the blood during the infusion is represented by a proportional increase in the detected MPI signal. This validates the ability of the detector to measure Fe blood concentration in the sensitive region of the detector. Fitting the small clearance-only time-periods between the injections in Fig. 5a with a 1st order clearance function suggests a clearance rate of 0.8 mg Fe/hr.

Notably, the raw data in Fig. 5a exhibits an increase in noise as the signal level increases. As this is not the case in the phantom data (Fig. 4), we infer that noise in the animal experiment is dominated by "physiological noise" at high signal levels. Figure 5b presents a deeper look into the noise behavior in three animal experiments. The scatter plot shows the changing noise level as a function of MPI signal magnitude during the SPIO infusions. To calculate the noise data points, the raw data was first high-pass filtered (cut-off at 0.2 Hz) to isolate the noise. Then, the plotted noise data points were calculated at each time point as the standard deviation of the previous 40 data points. A linear fit (dashed line) shows that the noise increases at a rate of 9.1 μmV noise/ 1V MPI signal. There is a baseline noise level of ~60 nV (solid line) below which thermal noise dominates and the noise level is independent of the signal level. The cross-over from thermal noise dominance to physiological noise dominance occurs at a signal level of ~3.2 μν in our experiments. For MPI signal levels above this baseline, the observed noise was proportional to the signal.

Figure 6 shows four cycles of the CO_2 responsivity experiment for rat #1. In this dataset a 1st order linear trend was removed (to remove baseline drift from SPIO clearance) and the data was low-pass filtered with a cutoff of 0.1 Hz. Hypocapnic, hypercapnic, and baseline time periods are shaded in light grey, dark grey, and white respectively. A blood gas analysis during a representative period of each state revealed 1) $paCO_2$ = 28 mmHg and paO_2 = 57 mmHg during hypocapnia, 2) $paCO_2$ = 49 mmHg and paO_2 = 47 mmHg during hypercapnia, 3) $paCO_2$ = 35 mmHg and paO_2 = 79 mmHg during baseline. The cerebral vasodilation during hypercapnia and vasoconstriction during hypocapnia led to changes in CBV which were readily observable as a 9.9% modulation in the MPI signal with a CNR of 50.

Figure 7 shows MPI CO_2 responsivity data for the three rats. The unfiltered MPI signal is plotted as a percent signal change for four cycles of hyper/hypocapnia for each animal, as well as the average of the four cycles. The average percent signal modulation in these three experiments was 9.6 ± 0.8%. The absolute signal level and noise level varied in the 3 experiments because of variations in the drive field amplitude, the remaining concentration of the SPIO in the blood at the time of the experiment, induced $\Delta paCO_2$, and detector positioning. The rat #1 experiment was performed with a drive field of 13 mT at the surface at the detector approximately 70 minutes post-infusion. The rat #2 experiment was performed with a drive field of 11 mT approximately 70 minutes post-infusion. The rat #3 experiment was performed with a drive field of 14 mT approximately 160 minutes post-infusion.

4. Discussion

The magnetic particle detector developed for measuring brain hemodynamic time-series yielded successful proof-of-concept results. Phantom experiments validated detection sensitivity to physiologically relevant SPIO concentrations and demonstrated the spatially limited sensitivity profile of the detector. *In vivo* rodent studies confirmed high sensitivity to CBV changes and also revealed a dominant noise component that was signal-level dependent.

Although high CNR CO_2 responsivity was measured with the single-sided detector, the percent signal change seen (~10%) was smaller than a previous MRI experiment with up to 55% signal change [1]. One contributing factor is discrepancies in the amplitude of the CO_2 blood gas modulation ($\Delta paCO_2$), which may differ based on ventilation settings and the time period of hypercapnia intervals. We observed an induced $\Delta paCO_2$ = 21 mmHg in rat #1, while Mandeville et al. induced a $\Delta paCO_2$ = 30 mmHg, which is expected to lead to a greater CBV change. The sensitivity profile of the detector is also a contributing factor to the expected percent signal change. The most sensitive region of the detector was positioned on scalp over the sagittal sinus of the rat (Fig. 3), which might have contributed a high baseline signal component that is minimally modulated by hypercapnia compared to the brain. This effect could easily be excluded with an MPI imaging device, where specific ROIs could be analyzed within the brain. Additionally, the observed smaller CBV modulation might arise from incomplete manipulation of the applied gasses through the animal “breathing around” the respirator.

The noise characteristics of the MPI time-series suggest a potential limiting factor to CNR. The noise in MPI measurements is typically considered to arise from the losses in the receiver coil and preamplifier (there is little “body loss noise” at the 75 kHz detection frequency [21]). For these thermal sources, the noise power level is proportional to the total resistive loss which is independent of the signal strength. Thus, time-series variance from thermal noise sources ($\sigma_{thermal}^2$) conventionally seen in MRI and MPI are constant. However, fMRI time-series are well known to be dominated by “physiological noise” (σ_{phys}^2), which is perhaps more correctly described as “signal clutter” rather than true noise. It arises from variance from uncontrolled modulations of the signal by poorly described physiological factors and intrinsic fluctuations in brain activity. Therefore, it looks like “noise” but is actually a complicated physiological modulation of the signal amplitude that contains a neural contribution. Since it is a modulation of the signal, this noise source, σ_{phys}, is routinely seen to vary in proportion to the signal level and in fMRI, its relative dominance can be controlled by the imaging parameters [22], [23]. Importantly, much of this variance derives from hemodynamic fluctuations, the spatial correlations of which have been shown to identify “functional connectivity” within the brain [24], [25]. Thus, physiological noise in a detected time-series can have positive as well as negative attributes. While the observation of a physiological noise component in the MPI time-course motivates further investigation, it by no means demonstrates the feasibility of resting-state functional connectivity experiments. Resting state connectivity would require that the observed physiological noise contains a sizable hemodynamic component of neuronal metabolic origin. However other, less interesting, sources such as respiration and cardiac pulsations can modulate the detected

signal time-course to produce noise-like fluctuations which also increases in proportion to the signal level similar to the observed effect.

A considerable portion of the high CNR observed in the hypercapnia experiments can be attributed to the large sensitive region of our coil-localized detection circuit, with a sensitive volume equivalent to a ~6.5mm cube. In contrast fMRI studies in rodents would typically have a spatial resolution below 1mm; a sensitive volume about 275 fold smaller. However, the dominance of physiological noise in fMRI experiments (and possibly in fMPI experiments) complicates the comparison of acquisitions at different voxel volumes. The CNR of an fMRI acquisition is determined by the temporal Signal to Noise Ratio (tSNR) of the time series. For many acquisitions, the time-series is physiological noise dominated and increasing signal levels by using coarser image resolution does not translate to significant improvement in tSNR (and thus functional CNR). For example increasing the voxel volume of a human 7T, 32 ch fMRI study from $1\times1\times3$ mm^3 to $5\times5\times3$ mm^3 (25 fold volume increase) yielded a tSNR increase of only about a factor of 1.8 [26]. In Kruger's original study [22], he determines that the asymptotic limit for grey matter tSNR is about 83, suggesting that increasing the voxel volume to very large detected regions will not improve the tSNR beyond this value. For a hypercapnia signal modulation of 20%, this yields a maximum "large voxel" CNR of about 17 for human MRI. To correctly estimate the relative sensitivity of the two modalities will require a full characterization of the fMPI physiological noise, followed by validation with similar resolution acquisitions.

One of the most promising opportunities for improvement in MPI-based hemodynamic measurements is development of better SPIO agent. Larger core SPIO nanoparticles contribute to higher MPI signal amplitude and could lead to improvements in image resolution due to a steep/high saturation level of the magnetization curve. However, relaxation effects counteract these potential improvements in large particles [27]. In addition, our functional neuroimaging application requires a blood-pool agent with a long blood half-life, and larger particles tend to be cleared faster. Optimized nanoparticles for MPI, which are not currently commercially available, potentially could yield significant improvements in MPI imaging characteristics.

The MPI signal can also be modulated by the coil-body distance of either the drive or receiver coil. If these distances systematically change in a manner correlated to the induction of hypercapnia, some or all of the signal change attributed to hypercapnia might be spurious. We do not have any specific measurements on this possible effect, but note that the problem is similar to that faced in MRI hypercapnia measurement's where a local transmit and receiver coil is similarly fixed above the rodent's head.

Although a CBV change directly alters the particle concentration and thus detected MPI signal level, particle relaxation effects can also modulate the signal. The response of the particles to the applied field is modulated by magnetic relaxation effects. If the reorientation of the particle magnetization arises from the physical rotation of the particle (Brownian relaxation), the process is expected to be sensitive to both the temperature and viscosity of the surrounding environment. In contrast, if the reorientation of the particle magnetization occurs due to internal re-alignment without rotation (Neel relaxation), the effect is mainly

dependent on temperature. In both cases, the sluggishness of the magnetization response can decrease sensitivity [28]. For example, in the presence of a very long re-orientation time constant no MPI response is seen at all. The relaxation effects also adversely affect image resolution. Thus, signal changes resulting from task-correlated modulations of temperature or viscosity could mimic hemodynamic changes, and relaxation effects can negatively impact MPI sensitivity and spatial resolution.

Relaxation times increase as a function of the particle size for both mechanisms and for the Brownian mechanism, the hydrodynamic diameter of the particle is important. The MPI sensitivity and spatial resolution for particles with core sizes in the 18 −32nm range (a typical range for MPI detection, including our 25nm core) were experimentally determined by Tay et al [29]. They showed that the spatial PSF for 24.4nm core particles (41nm hydrodynamic core) was approximately twice that expected without relaxation and even greater blurring occurred for larger particles. Even so, the 24.4nm particle provided the best combination of detectability and PSF of the particles detected.

Our study did not localize the MPI signal beyond the detector sensitivity region of the Faraday detectors, and a full tomographic study is needed to assess the hemodynamic sensitivity as a function of detection volume (voxel volume) similar to those done for human MRI [22]. A future extension of the presented MP detector to a tomographic imaging system will allow for fMPI mapping experiments in this rodent model, including somatosensory (forepaw or whisker) or visual stimulation and study of sensitivity as a function of voxel volume. Although forepaw stimulation was attempted with the presented detector, we believe that fCBV in the somatosensory cortex was obscured by the large baseline signal from non-activated brain regions as well as the scalp and sagittal sinus (as described above). Thus, the ability to create a full map or at least localize somatosensory cortex using a selection field will be required to perform fMPI activation studies of focally responding brain regions. In addition to focal fMPI experiments, pharmacological experiments [30], which restrict averaging and thus place a premium on intrinsic CNR, might potentially benefit from MPI.

Functional imaging with MPI faces several barriers and downsides compared to other modalities. Firstly, it requires the injection of an agent, which will limit its use in many experiments and introduces regulatory barriers. There are currently only a few iron oxide nanoparticle agents approved for human use. Secondly, the availability of tomographic MPI scanners, while reported by multiple groups, and now commercially available for rodents, are not as widely available or as flexible in their ability to trade-off sensitivity, imaging speed and spatial resolution as current MRI scanners and, of course, a human MPI scanner has yet to be demonstrated so sensitivity and resolution estimates for human fMPI are even further from validation.

5. Conclusion

We present a single-sided Magnetic Particle detector used for fCBV measurement in rats. Experiments with the detector yielded dynamic measurements of brain hemodynamics using the principles of MPI. Even with the limited sensitivity volume of the single-sided detector,

a robust 10% signal change was observed with a CNR of 50 during hyper/hypocapnia modulation. This serves as a proof-of-concept experiment that motivates the future design of full tomographic imaging systems dedicated to small animal functional neuroimaging with MPI.

Supplementary Material

Refer to Web version on PubMed Central for supplementary material.

Acknowledgements

This work was supported by the Institute for Mental Health of the National Institutes of Health under award number R24MH106053. The content is solely the responsibility of the authors and does not necessarily represent the official views of the National Institutes of Health. Thank you to the groups of S. Conolly at UC Berkeley and M. Griswold at Case Western for advice on MPI system development, Suma Anand and Charlotte Sappo for assistance with filter design, and Simon Siglovsky, Christopher Ha, Charlotte Sappo, and Elizabeth Choi for assistance with mechanical components of the detector system.

References:

[1]. Mandeville JB et al., “Dynamic functional imaging of relative cerebral blood volume during rat forepaw stimulation,” Magn. Reson. Med, vol. 39, no. 4, pp. 615–624, Apr. 1998. [PubMed: 9543424]

[2]. Vanduffel W et al., “Visual Motion Processing Investigated Using Contrast Agent-Enhanced fMRI in Awake Behaving Monkeys,” Neuron, vol. 32, no. 4, pp. 565–577, Nov. 2001. [PubMed: 11719199]

[3]. Leite FP et al., “Repeated fMRI Using Iron Oxide Contrast Agent in Awake, Behaving Macaques at 3 Tesla,” NeuroImage, vol. 16, no. 2, pp. 283–294, Jun. 2002. [PubMed: 12030817]

[4]. Van Camp N, Peeters RR, and Van der Linden A, “A comparison between blood oxygenation level- dependent and cerebral blood volume contrast in the rat cerebral and cerebellar somatosensoric cortex during electrical paw stimulation,” J. Magn. Reson. Imaging JMRI, vol. 22, no. 4, pp. 483–491, Oct. 2005.

[5]. Mandeville JB et al., “Exogenous contrast agent improves sensitivity of gradient-echo functional magnetic resonance imaging at 9.4 T,” Magn. Reson. Med, vol. 52, no. 6, pp. 1272–1281, Dec. 2004. [PubMed: 15562489]

[6]. Qiu D, Zaharchuk G, Christen T, Ni WW, and Moseley ME, “Contrast-Enhanced Functional Blood Volume Imaging (CE-fBVI): Enhanced Sensitivity for Brain Activation in Humans using the Ultrasmall Superparamagnetic Iron Oxide Agent Ferumoxytol,” NeuroImage, vol. 62, no. 3, pp. 1726–1731, Sep. 2012. [PubMed: 22584230]

[7]. Baumgartner R et al., “Evaluation of an fMRI USPIO-based assay in healthy human volunteers,” J. Magn. Reson. Imaging, vol. 46, no. 1, pp. 124–133, Jul. 2017. [PubMed: 27775841]

[8]. D’Arceuil H et al., “Ferumoxytol enhanced resting state fMRI and relative cerebral blood volume mapping in normal human brain,” NeuroImage, vol. 83, pp. 200–209, Dec. 2013. [PubMed: 23831413]

[9]. Zhao F, Wang P, Hendrich K, and Kim S-G, “Spatial specificity of cerebral blood volume-weighted fMRI responses at columnar resolution,” NeuroImage, vol. 27, no. 2, pp. 416–424, Aug. 2005. [PubMed: 15923128]

[10]. Fukuda M, Moon C-H, Wang P, and Kim S-G, “Mapping iso-orientation columns by contrast agent-enhanced functional magnetic resonance imaging: reproducibility, specificity, and evaluation by optical imaging of intrinsic signal,” J. Neurosci. Off. J. Soc. Neurosci, vol. 26, no. 46, pp. 11821–11832, Nov. 2006.

[11]. Mandeville JB and Marota JJ, “Vascular filters of functional MRI: spatial localization using BOLD and CBV contrast,” Magn. Reson. Med, vol. 42, no. 3, pp. 591–598, Sep. 1999. [PubMed: 10467305]

[12]. Zheng B, Vazin T, Goodwill PW, Conway A, Verma A, Saritas EU, Schaffer D, Conolly SM. Magnetic Particle Imaging tracks the long-term fate of in vivo neural cell implants with high image contrast. Sci Rep. 11;5: 14055 9 2015. doi: 10.1038/srep14055. PubMed PMID: 26358296; PubMed Central PMCID: PMC4566119.

[13]. Gleich B and Weizenecker J, "Tomographic imaging using the nonlinear response of magnetic particles," Nature, vol. 435, no. 7046, pp. 1214–1217, Jun. 2005. [PubMed: 15988521]

[14]. Buzug TM et al., "Magnetic particle imaging: Introduction to imaging and hardware realization," Z. Für Med. Phys, vol. 22, no. 4, pp. 323–334, Dec. 2012.

[15]. Goodwill PW and Conolly SM, "The X-space formulation of the magnetic particle imaging process: 1-D signal, resolution, bandwidth, SNR, SAR, and magnetostimulation," IEEE Trans. Med. Imaging, vol. 29, no. 11, pp. 1851–1859, Nov. 2010. [PubMed: 20529726]

[16]. Weizenecker J, Gleich B, and Borgert J, "Magnetic particle imaging using a field free line," J. Phys. Appl. Phys, vol. 41, no. 10, p. 105009, 2008.

[17]. Goodwill PW, Konkle JJ, Zheng B, Saritas EU, and Conolly SM, "Projection X-Space Magnetic Particle Imaging," IEEE Trans. Med. Imaging, vol. 31, no. 5, pp. 1076–1085, 5 2012. [PubMed: 22552332]

[18]. Mason EE, Cooley CZ, Cauley SF, Griswold MA, Conolly SM, and Wald LL, "Design analysis of an MPI human functional brain scanner," Int. J. Magn. Part. Imaging, vol. 3, no. 1, Mar. 2017.

[19]. Goto T, Hatanaka R, Ogawa T, Sumiyoshi A, Riera J, and Kawashima R, "An Evaluation of the Conductivity Profile in the Somatosensory Barrel Cortex of Wistar Rats," J. Neurophysiol, vol. 104, no. 6, pp. 3388–3412, Dec. 2010. [PubMed: 20810682]

[20]. Christen T et al., "High-resolution cerebral blood volume imaging in humans using the blood pool contrast agent ferumoxytol: High Resolution CBV Maps in Humans Using USPIOs," Magn. Reson. Med, vol. 70, no. 3, pp. 705–710, Sep. 2013. [PubMed: 23001902]

[21]. Myers W et al., "Calculated signal-to-noise ratio of MRI detected with SQUIDs and Faraday detectors in fields from 10μT to 1.5T," J. Magn. Reson, vol. 186, no. 2, pp. 182–192, Jun. 2007. [PubMed: 17337220]

[22]. Krüger G and Glover GH, "Physiological noise in oxygenation-sensitive magnetic resonance imaging," Magn. Reson. Med, vol. 46, no. 4, pp. 631–637, Oct. 2001. [PubMed: 11590638]

[23]. Triantafyllou C et al., "Comparison of physiological noise at 1.5 T, 3 T and 7 T and optimization of fMRI acquisition parameters," NeuroImage, vol. 26, no. 1, pp. 243–250, 5 2005. [PubMed: 15862224]

[24]. Biswal B, Yetkin FZ, Haughton VM, and Hyde JS, "Functional connectivity in the motor cortex of resting human brain using echo-planar MRI," Magn. Reson. Med, vol. 34, no. 4, pp. 537–541, Oct. 1995. [PubMed: 8524021]

[25]. Raichle ME, MacLeod AM, Snyder AZ, Powers WJ, Gusnard DA, and Shulman GL, "A default mode of brain function," Proc. Natl. Acad. Sci. U. S. A, vol. 98, no. 2, pp. 676–682, Jan. 2001. [PubMed: 11209064]

[26]. Triantafyllou C, Polimeni JR, and Wald LL, "Physiological noise and signal-to-noise ratio in fMRI with multi-channel array coils," NeuroImage, vol. 55, no. 2, pp. 597–606, Mar. 2011. [PubMed: 21167946]

[27]. Ferguson RM, Minard KR, and Krishnan KM, "Optimization of nanoparticle core size for magnetic particle imaging," J. Magn. Magn. Mater, vol. 321, no. 10, pp. 1548–1551, 5 2009. [PubMed: 19606261]

[28]. Weaver JB et al., "Quantification of magnetic nanoparticles with low frequency magnetic fields: compensating for relaxation effects," Nanotechnology, vol. 24, no. 32, p. 325502, 2013. [PubMed: 23867287]

[29]. Tay ZW, Hensley DW, Vreeland EC, Zheng B, and Conolly SM, "The relaxation wall: experimental limits to improving MPI spatial resolution by increasing nanoparticle core size," Biomed. Phys. Eng. Express, vol. 3, no. 3, p. 035003, 2017. [PubMed: 29250434]

[30]. Liu CH, Greve DN, Dai G, Marota JJA, and Mandeville JB, "Remifentanil administration reveals biphasic phMRI temporal responses in rat consistent with dynamic receptor regulation," NeuroImage, vol. 34, no. 3, pp. 1042–1053, Feb. 2007. [PubMed: 17169578]

HIGHLIGHTS:

- A single-sided Magnetic Particle (MP) detector was developed for rodent CBV measurements.
- Phantom experiments validated sensitivity to physiologically relevant SPIO concentrations.
- fCBV measurements during hyper/hypocapnia detected CBV modulations with CNR = 50.
- Observed physiological noise in the resting-state merits further study.

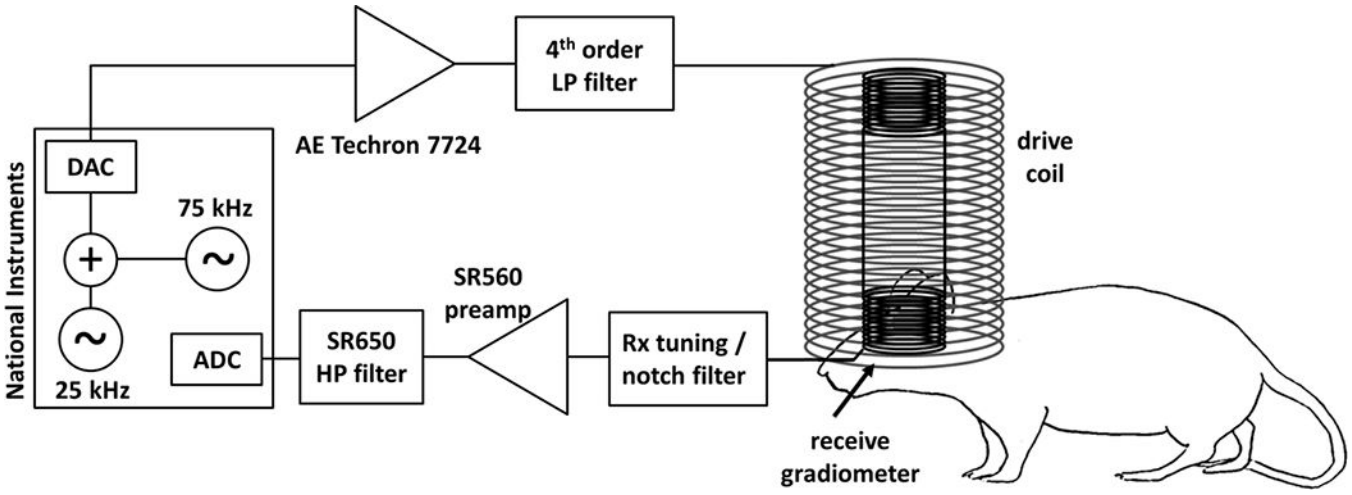

Figure 1:

Schematic of MPI single-sided detector. A National Instruments DAQ is used as console, generating a 25 kHz analog burst pulses for the drive field and digitizing the simultaneously measured MPI signal. An adjustable 75 kHz waveform is added to the 25 kHz output to cancel distortion generated in the drive chain. The drive field waveform is amplified (AE Techron 7224) and low-passed filtered before generating the AC drive field in the drive coil. The non-linear SPIO magnetization is picked-up by the nested gradiometer receiver coil, which is tuned to the 3rd harmonic (75 kHz) of the drive frequency. The front-end also includes a notch filter (to attenuates direct feedthrough of the drive field), a low-noise preamplifier (SR560), and an additional high-pass filter stage (SR650).

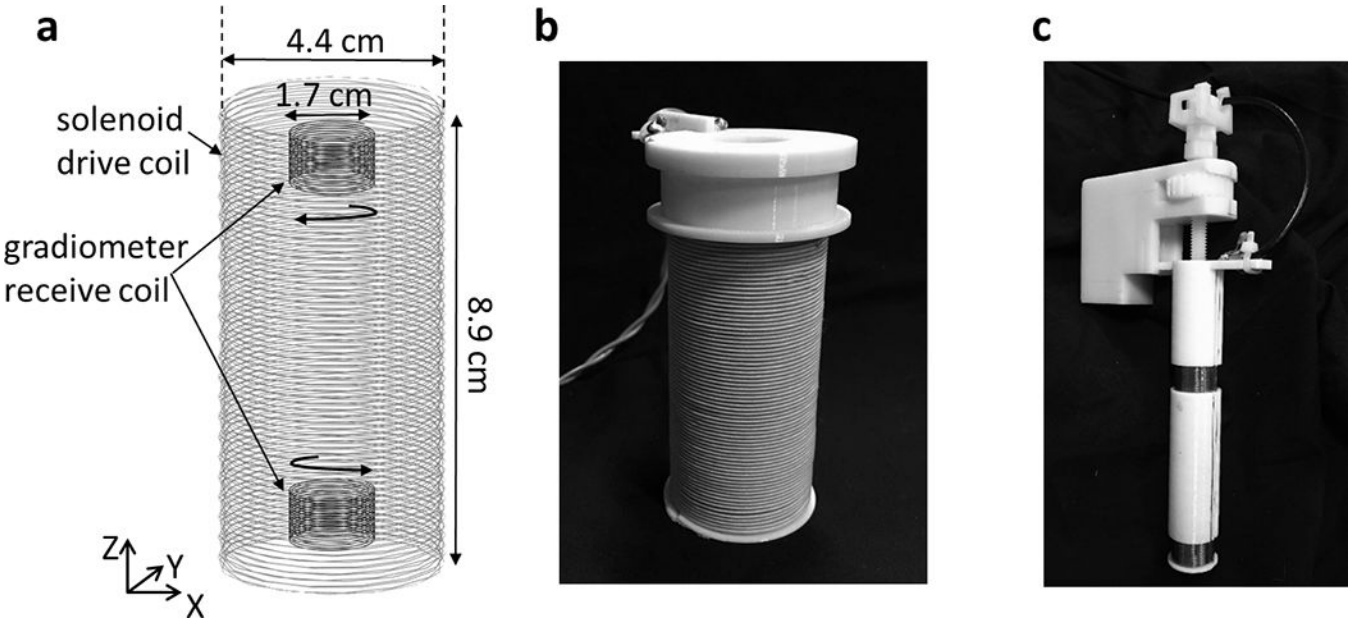

Figure 2:

a) Diagram of single-sided Magnetic Particle (MP) detector with solenoid drive coil and gradiometer receive coil. b) The solenoid drive coil made up of 2 layers of Litz wire with a total of 145 windings. The coil produces 1 mT/A at the surface of the detector. c) The gradiometer receiver coil has two 40-turn, 1 cm sections wound in opposite directions to attenuate direct feedthrough of the drive field. Careful positioning of the gradiometer attenuates the drive field feedthrough up to 80 dB.

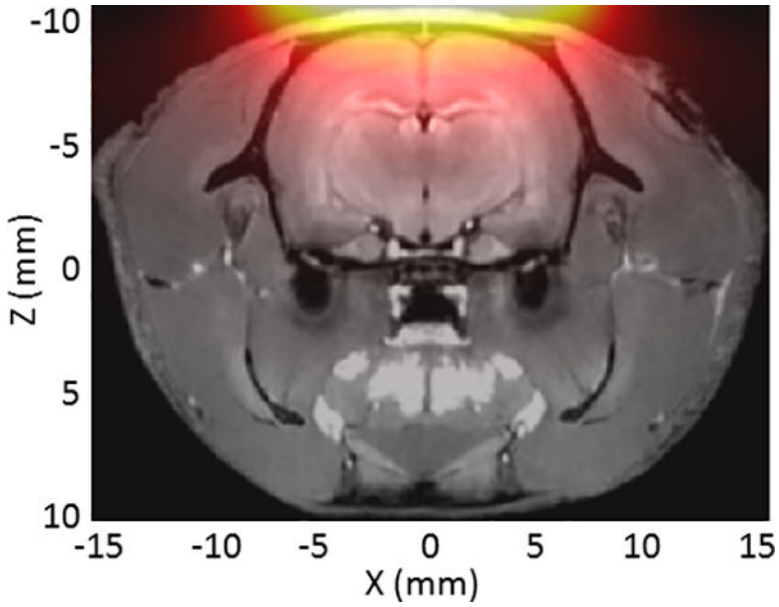

Figure 3:

Simulated sensitivity map under surface of the single-sided detector overlaid on a T1-weighted MRI image of a rat head. The sensitivity map was produced by simulating the acquired the 3rd harmonic signal for discrete SPIO samples at each location. The volume of the brain weighted by the sensitivity profile of the detector is about 24% percent of the full brain volume.

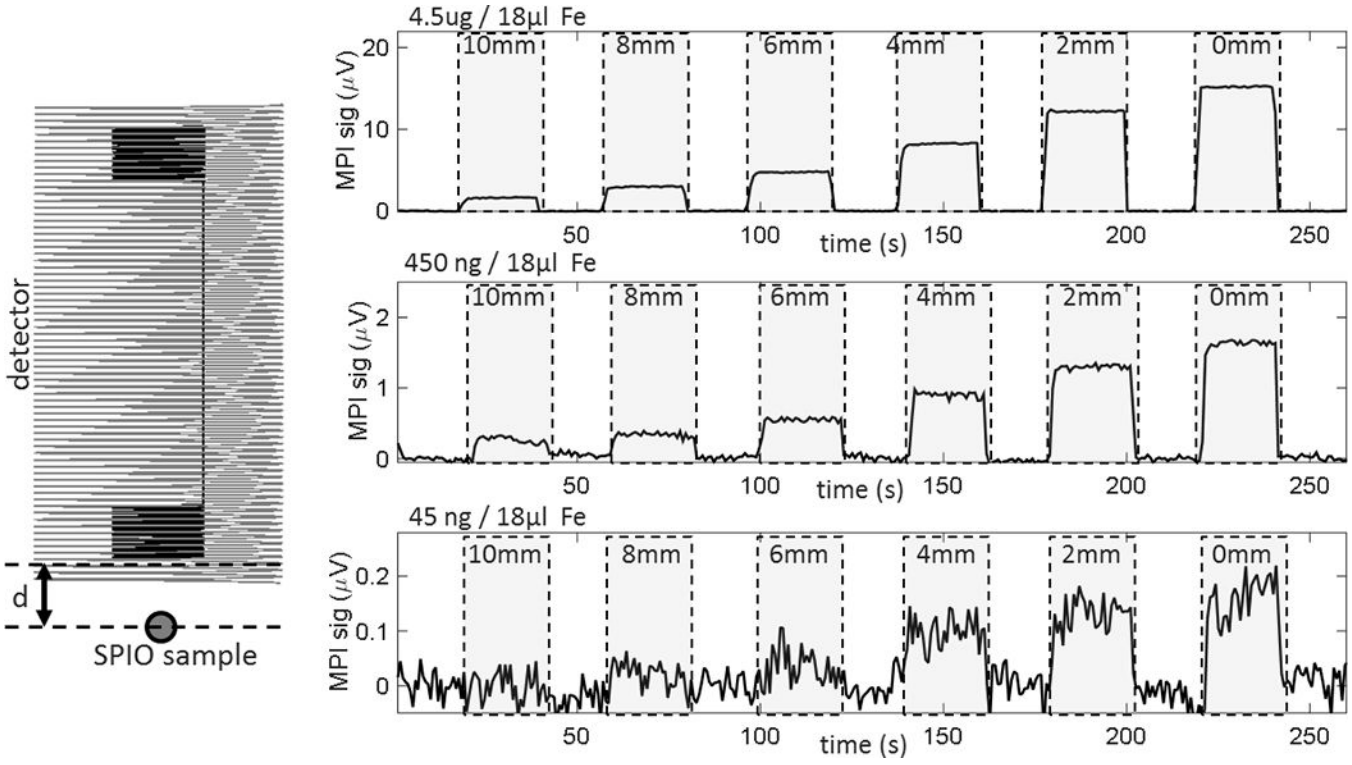

Figure 4:

Plots show detection capability of the MP detector in relation to the distance between the detector surface and SPIO sample (d). The 3rd harmonic signal change is shown when sample is moved to 10 mm, 8 mm, 6 mm, 4 mm, 2 mm, and 0 mm away from the end of the detector (in between, sample is removed from detectable area). The phantom holds 18 µL bulbs containing 4.5 µg, 450 ng, and 45 ng Fe in H20 solution. The lowest concentration sample (45 ng Fe) is lower than the expected Fe change from a 25% neuroactivation-induced CBV change in a 3mm voxel (52 ng). At the surface of the detector (d = 0 mm), this concentration was detected with an SNR of 5.4. Each point represents the 75 kHz signal component from a 16 ms integration time.

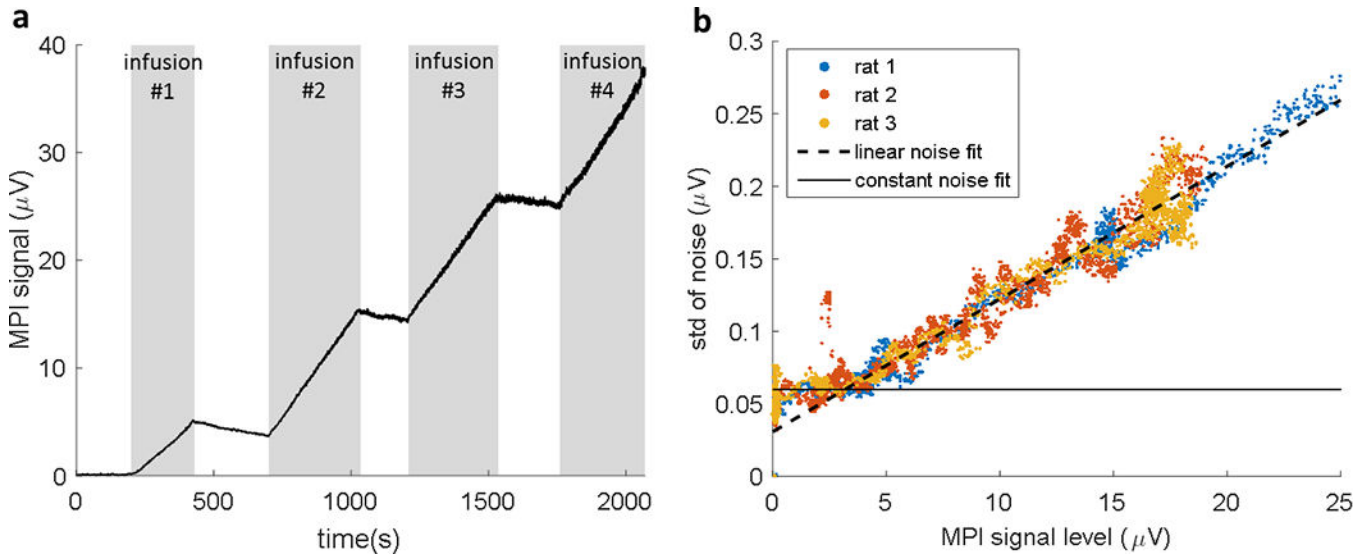

Figure 5:

a) *in vivo* MPI data (at baseline CO_2 levels) from the single-sided detector is shown during four 1.4 mg Fe infusions at a rate of 7 mg [Fe]/hr. During the infusions the measured MPI signal (3rd harmonic) from the detector's sensitivity volume increases proportionally with the concentration of SPIO in the blood. The signal increase during infusions 2–4 was 11.6±0.05 μV, while infusion #1 yielded a signal increase of 5.1 μV (about 56% of SPIO was lost in the line). A notable increase in noise is presented as the signal increases. b) The standard deviation of the noise is shown as a function of MPI signal level. Each data point represents the standard deviation in 40 time-series points during the SPIO infusion in 3 rats. The linear increase in noise with signal strength is a characteristic of signal modulation by uncontrolled physiological processes, commonly called "physiological noise" in the fMRI literature. The noise appears to be physiological noise dominated above MPI signal level = 3.2 μν.

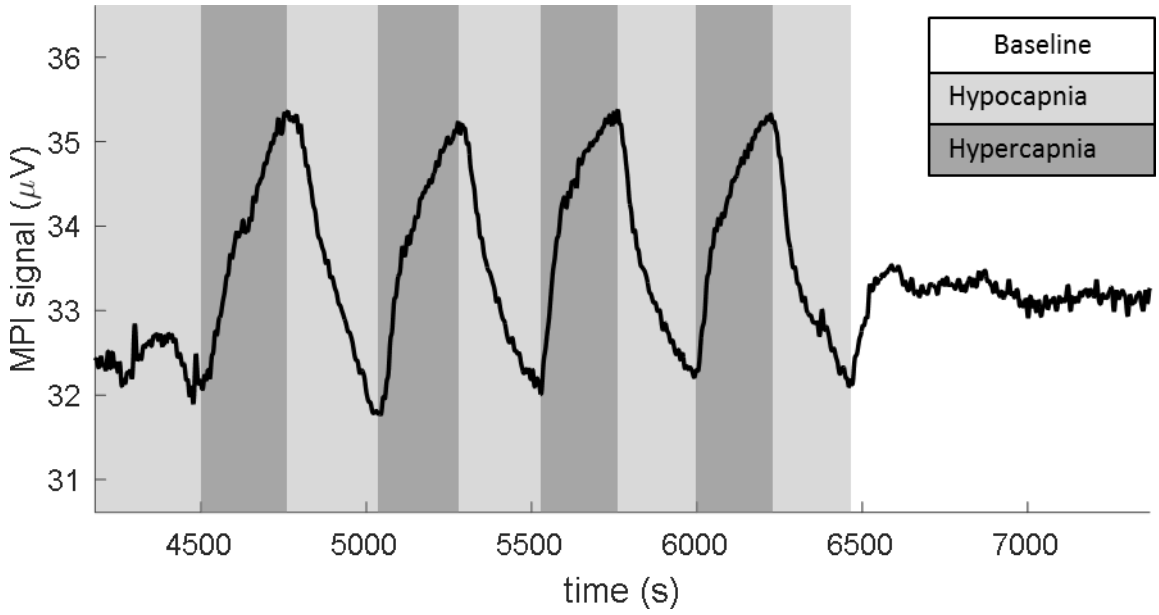

Figure 6:

MPI measurement of fCBV modulated by hypercapnic paradigm in a rat model. The drive field at the surface of the detection was a 25 kHz sinusoid at 14 mT. The 3rd harmonic (75 kHz) response of the particles is shown. A 1st order linear trend was removed from the data and the digital low-pass filter with fc = 0.1 Hz was applied. Ventilation properties controlled for alternating hypo/hypercapnia in 5 min. periods. The MPI signal shows a 9.9% signal modulation with the expected CBV trend and CNR = 50. Representative blood-gas measurements were recorded for each condition: Hypocapnia: resp rate = 55 BPM, $paCO_2$ = 28 mmHg, paO_2 = 57 mmHg. Hypercapnia: resp rate = 32 BPM with 5% CO_2 gas mixture paCO2 = 49 mmHg, paO2 = 47 mmHg. Baseline: resp rate = 34 BPM, $paCO_2$ = 35 mmHg, paO2 = 79 mmHg.

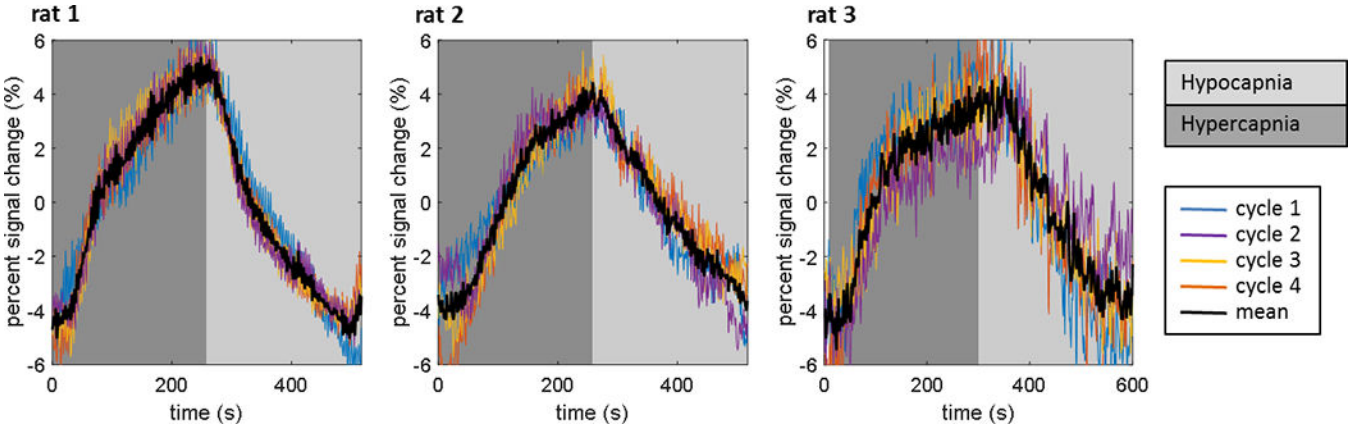

Figure 7:

Data from the hypo/hypercapnia experiment (Fig. 6) repeated in 3 animals with different drive field amplitudes (13 mT for rat 1, 11 mT for rat 2, and 14 mT for rat 3). Four raw data cycles are overlaid as well as the mean data for each animal. The Fe concentration in the blood varies for each animal based on the timing of the experiment post-infusion (~70 min for rat 1, ~70 min for rat 2, ~160 min for rat 3). The absolute signal level and noise varies for the different experiments based on the drive field amplitude, SPIO concentration in the blood, detector positioning, and $\Delta paCO_2$. However, a percent signal change of 8–10% was observed in all experiments.